Original article

MOLECULAR METABOLISM

Conditional deletion of CEACAM1 in hepatic stellate cells causes their activation

Harrison T. Muturi[1,10], Hilda E. Ghadieh[1,2,10], Suman Asalla[1,10], Sumona G. Lester[3], Getachew D. Belew[1], Sobia Zaidi[1], Raziyeh Abdolahipour[1], Abhishek P. Shrestha[4], Agnes O. Portuphy[1], Hannah L. Stankus[1], Raghd Abu Helal[1], Stefaan Verhulst[5], Sergio Duarte[4], Ali Zarrinpar[4], Leo A. van Grunsven[5], Scott L. Friedman[6], Robert F. Schwabe[7], Terry D. Hinds Jr.[8], Sivarajan Kumarasamy[1], Sonia M. Najjar[1,9,*]

ABSTRACT

Objectives: Hepatic CEACAM1 expression declines with advanced hepatic fibrosis stage in patients with metabolic dysfunction-associated steatohepatitis (MASH). Global and hepatocyte-specific deletions of *Ceacam1* impair insulin clearance to cause hepatic insulin resistance and steatosis. They also cause hepatic inflammation and fibrosis, a condition characterized by excessive collagen production from activated hepatic stellate cells (HSCs). Given the positive effect of PPARγ on CEACAM1 transcription and on HSCs quiescence, the current studies investigated whether CEACAM1 loss from HSCs causes their activation.

Methods: We examined whether lentiviral shRNA-mediated CEACAM1 donwregulation (KD-LX2) activates cultured human LX2 stellate cells. We also generated *LratCre* + $Cc1^{fl/fl}$ mutants with conditional *Ceacam1* deletion in HSCs and characterized their MASH phenotype. Media transfer experiments were employed to examine whether media from mutant human and murine HSCs activate their wild-type counterparts.

Results: *LratCre* + $Cc1^{fl/fl}$ mutants displayed hepatic inflammation and fibrosis but without insulin resistance or hepatic steatosis. Their HSCs, like KD-LX2 cells, underwent myofibroblastic transformation and their media activated wild-type HSCs. This was inhibited by nicotinic acid treatment which blunted the release of IL-6 and fatty acids, both of which activate the epidermal growth factor receptor (EGFR) tyrosine kinase. Gefitinib inhibition of EGFR and its downstream NF-κB/IL-6/STAT3 inflammatory and MAPK-proliferation pathways also blunted HSCs activation in the absence of CEACAM1.

Conclusions: Loss of CEACAM1 in HSCs provoked their myofibroblastic transformation in the absence of insulin resistance and hepatic steatosis. This response is mediated by autocrine HSCs activation of the EGFR pathway that amplifies inflammation and proliferation.

Keywords Hepatic fibrosis; Inflammation; Hepatic steatosis; Stellate cell proliferation; Retinoic acid

1. INTRODUCTION

Metabolic dysfunction-associated steatotic liver disease (MASLD), formerly termed non-alcoholic fatty liver disease, currently represents the most common cause of chronic liver disease worldwide [1]. MASLD spans a broad spectrum of metabolic disease with hepatic fibrosis defining its most aggressive form, Metabolic dysfunction-associated steatohepatitis (MASH), together with inflammation, hepatocyte damage, and apoptosis. Hepatic fibrosis is on the rise and currently constitutes a leading etiology in patients with MASH, partly because of limited targeted therapy [2,3]. This necessitates the need for further studies exploring its molecular and cellular basis.

Histologically, hepatic fibrosis in patients with MASH is characterized by early lesions of perisinusoidal collagen deposition, followed by portal and eventually, bridging fibrosis [4]. It implicates the activation of hepatic stellate cells (HSCs) located in the Space of Disse between liver sinusoidal endothelial cells (LSECs) and hepatocytes. HSCs represent approximately 10% of resident liver cells. In healthy liver, PPARγ activation maintains HSCs quiescent and containing large lipid droplets filled with vitamin A as retinyl esters (RE), triacylglycerols (TG) and cholesteryl esters (CE) [5]. Following transdifferentiation into proliferative, contractile, inflammatory myofibroblasts with enhanced extracellular matrix (ECM) production, HSCs lose their retinoid content [6]. This is associated with reduced PPARγ and reciprocal elevation in

[1]Department of Biomedical Sciences, Heritage College of Osteopathic Medicine, Ohio University, Athens, OH, USA [2]Department of Biomedical Sciences, University of Balamand, Faculty of Medicine and Health Sciences, Al-Koura, Lebanon [3]Center for Diabetes and Endocrine Research, College of Medicine and Life Sciences, University of Toledo, Toledo, OH, USA [4]Department of Surgery, College of Medicine, University of Florida, Gainesville, FL, USA [5]Liver Cell Biology Research Group, Vrije Universiteit Brussel, Brussel, Belgium [6]Division of Liver Diseases, Icahn School of Medicine at Mount Sinai, New York 10029, NY, USA [7]Department of Medicine and the Digestive and Liver Disease Research Center, Columbia University New York, NY, USA [8]Department of Pharmacology and Nutritional Sciences, University of Kentucky College of Medicine, Lexington, KY, USA [9]Diabetes Institute, Heritage College of Osteopathic Medicine, Ohio University, Athens, OH, USA

[10] Harrison T. Muturi, Hilda E. Ghadieh and Suman Asalla contributed equally to these studies.

*Corresponding author. Heritage College of Osteopathic Medicine; Irvine Hall, 1 Ohio University; Athens, OH 45701-2979, USA. E-mail: najjar@ohio.edu (S.M. Najjar).

Received February 22, 2024 • Revision received July 24, 2024 • Accepted August 9, 2024 • Available online 19 August 2024

https://doi.org/10.1016/j.molmet.2024.102010

Abbreviations

CEACAM1	Carcinoembryonic Antigen-related Cell Adhesion Molecule 1 protein in mice and humans
CEACAM1	Human gene encoding CEACAM1 proteins
Ceacam1	Gene encoding CEACAM1 protein in mice
LratCre + *Cc1*$^{fl/fl}$	Stellate cell-specific *Ceacam1* mutants
LratCre − *Cc1*$^{+/+}$	Wild-type controls
LratCre + *Cc1*$^{+/+}$	*LratCre* controls
LratCre − *Cc1*$^{fl/fl}$	*Ceacam1* Floxed controls
HSCs	Hepatic Stellate Cells
KD-LX2	LX2 human hepatic stellate cell line with shRNA-mediated suppression of CEACAM1
Scr-LX2	Control LX2 cell line with scramble RNA

the level of PPARβ/δ [7,8], which could be activated by all trans-retinoic acid [9] and PUFA [10] to increase HSCs proliferation via inducing the p38 and JNK MAPK pathways [8]. Further studies are needed to fully identify the factors that cause HSCs activation [11].

Virtually every liver cell contributes to HSCs activation, and they all express the Carcinoembryonic Antigen-related Cell Adhesion Molecule 1 (CEACAM1), with a dominant expression in hepatocytes where it promotes insulin clearance. Depletion of *Ceacam1* gene globally [12] or exclusively in hepatocytes [13], causes chronic hyperinsulinemia, emanating chiefly from reduced insulin clearance, followed by hepatic insulin resistance, steatohepatitis and visceral obesity. It also provokes HSCs activation and a characteristic MASH-like fibrosis [14,15]. Fed a high-fat diet, mice lacking CEACAM1 in hepatocytes develop advanced hepatocellular injury accompanied by chicken-wire fibrosis and apoptosis [14,16]. Reciprocally, liver-specific rescuing of CEACAM1 reverses metabolic dysregulation and hepatic fibrosis in global *Cc1*$^{-/-}$ null mice [14]. In contrast, CEACAM1 loss in endothelial cells promotes hepatic fibrosis, driven by increased production of endothelin1, without insulin resistance or hepatic steatosis [17]. Consistent with these data in genetically-modified mice, patients with MASH exhibit a progressive loss of CEACAM1 in liver [15] and particularly in LSECs [17] as the disease advances.

CEACAM1 is also expressed in pericytes [18], including HSCs [19]. Herein we investigated whether its loss of CEACAM1 in HSCs induces their activation and sought to uncover underlying mechanisms.

2. MATERIALS AND METHODS

2.1. Generation and metabolic phenotyping of *LratCre* + *Cc1*$^{fl/fl}$ mice

As detailed in Supplemental data, *Cc1*$^{loxp/loxp}$ mice were crossed with *LratCre* transgenic mice expressing a Cre recombinase driven by mouse lecithin-retinol acyltransferase (Lrat) promoter [20]. Stellate cell-specific deletion of *Ceacam1* in C57BL/6Jxhomozygotes (*LratCre* + *Cc1*$^{fl/fl}$) was confirmed by PCR reaction using gene-specific primers (Fig. S1). As littermate controls, this study used homozygotes of wild-type *Ceacam1* allele with (*LratCre* + *Cc1*$^{+/+}$) or without *Cre* (*LratCre* − *Cc1*$^{+/+}$), and homozygotes of *Ceacam1*-floxed allele without *Cre* (*LratCre* − *Cc1*$^{fl/fl}$) to rule out potential confounding effects of floxing and introducing *Cre* recombinase.

Per institutionally approved protocols, animals were housed in a 12-h dark-light cycle and fed standard chow *ad libitum*. Male mice were kept in cages with Alpha-dri bedding before undergoing metabolic phenotyping [intraperitoneal (IP) glucose and insulin tolerance tests-GTT and ITT, respectively]. Following recovery, mice were fasted for 18 h, anesthetized with an IP injection of pentobarbital (1.1 mg/kg BW), and their retro-orbital venous blood was drawn and tissues extracted for biochemical evaluation (Supplemental data).

2.2. Liver histology and immunohistochemical analysis

As detailed in Supplemental data, fixed liver sections were stained with hematoxylin-eosin (H&E) or with 0.1% Sirius Red stain to evaluate hepatic fibrosis. Images were taken using Nikon Eclipse 90i Microscope and 10 randomly selected high power fields (20×) per sample were imaged with ImageJ (v1.53t) to quantify Sirius Red stain as % area [17]. For immunohistochemical (IHC) analysis, liver sections underwent antigen-retrieval, blocking with rabbit or mouse serum, stained overnight at 4 °C with specific antibodies, blotted with species-specific biotinylated secondary antibodies before being hematoxylin-counterstained [17]. Images were taken using Nikon Eclipse 90i Microscope and evaluated blindly to count positively stained cells in 5 fields/mouse at 40× magnification.

2.3. Determination of CEACAM1 levels in human HSCs

Human HSC RNA expression values for CEACAM1 were obtained from El Taghdouini et al., GSE68001 [21]. In that study, cells were isolated from healthy donor tissue; briefly, quiescent HSCs (qHSCs) were sorted as CD32−CD45−UV+ cells using a FASCAria (BD Biosciences, San Jose, CA). Activated HSCs (aHSCs) were obtained by plating qHSCs in DMEM (Gibco) supplemented with 20% FBS, and after two days in DMEM with 10% FBS. Microarray data was imported and normalized in RStudio using the Affy R package. The expression of CEACAM1 was extracted from the dataset and imported in Graphpad Prism as normalized CEACAM1 expression.

2.4. Media transfer experiments in primary murine hepatic stellate cells

Primary HSCs were isolated from ≥8-month-old control *LratCre* − *Cc1*$^{fl/fl}$ (recipient cells) and mutant mice *LratCre* + *Cc1*$^{fl/fl}$ (donor cells) [22]. Cells were cultured in 12-well-plates for 5−10 days. *LratCre* + *Cc1*$^{fl/fl}$ donor cells were washed twice and incubated in phenol red-free DMEM-10% FBS media before treating with nicotinic acid (NA, 500 μM) (Sigma−Aldrich) or buffer alone for 24 h. Media were collected, centrifuged at 380 xg for 3 min to remove cell debris and the "conditioned media" were transferred to the twice-washed *LratCre* − *Cc1*$^{fl/fl}$ recipient HSCs. 24 h later, cells were lysed for mRNA analysis (see below). In some experiments, 10 μM Gefitinib (Sigma−Aldrich), an EGFR tyrosine kinase inhibitor [23], or dimethyl sulfoxide (DMSO-vehicle) were added to recipient cells for additional 24 h before cell lysis. Media levels of fatty acids (NEFA-C enzymatic colorimetric assay; Wako, Richmond, VA), interleukin-6 (ELISA Kit, ab222503, Abcam) and TNFα (ELISA Kit, ab100747, Abcam) were determined per manufacturer instructions [17].

2.5. Experiments with LX2 cells with stable downregulation of human CEACAM1 expression

The immortalized human hepatic stellate LX2 cell line was infected with a human CEACAM1 shRNA lentiviral construct to establish a KD line with stable knockdown of hCEACAM1 and scramble control (Scr), as detailed in Supplemental data.

For lipid analysis, KD-LX2 and Scr-LX2 cells were seeded in 6-well-plates (4×10^4 cells/well) for 48 h before being stained with Nile Red (Sigma−Aldrich) and evaluated with densitometry by Image J software to measure lipid content [24]. Media was collected to determine free glycerol levels using Glycerol Assay Kit (BioVision, Milpitas, CA) [24]. Media transfer from KD-LX2 to Scr-LX2 controls was performed as above and levels of fatty acids (NEFA-C enzymatic colorimetric assay;

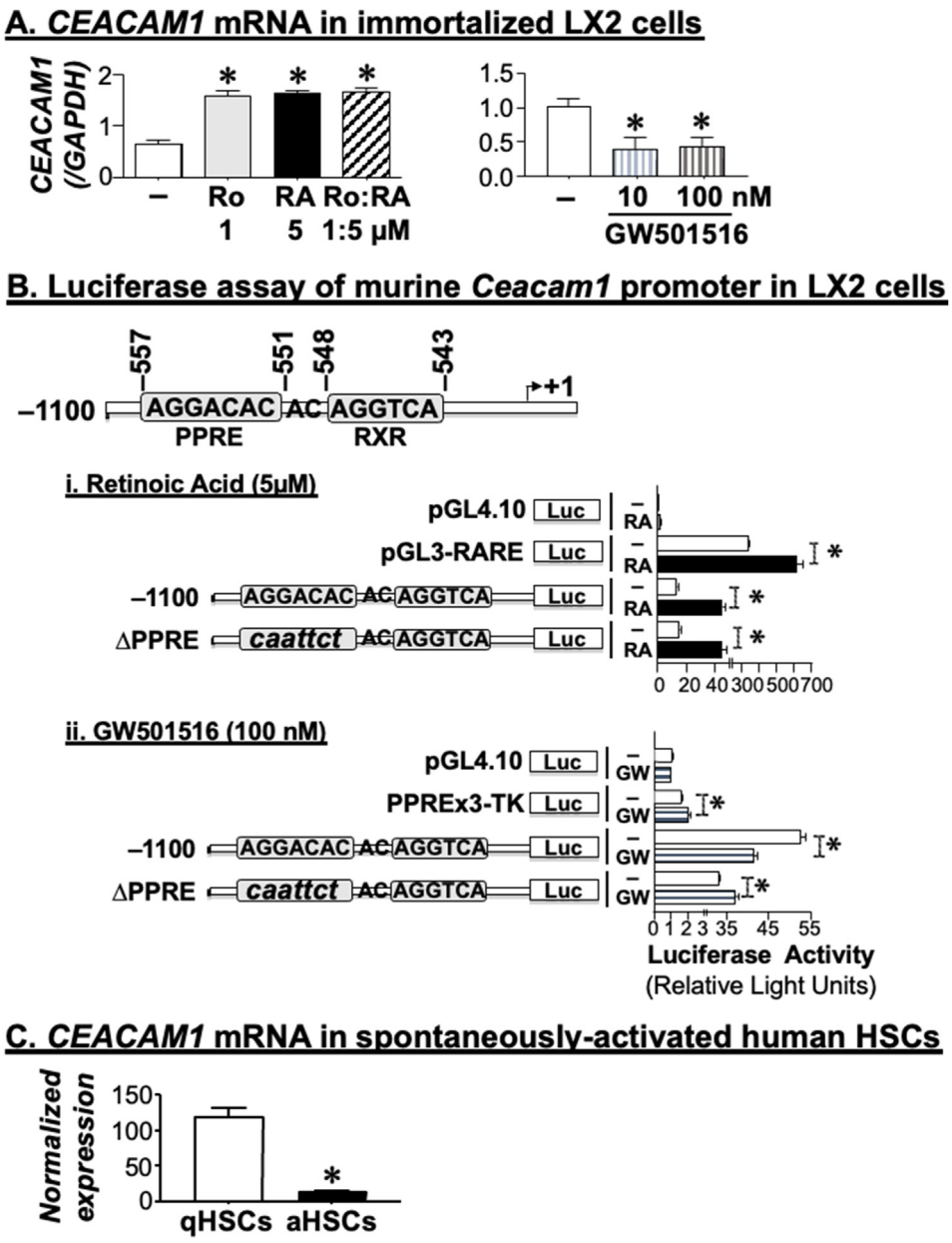

Figure 1: Regulation of CEACAM1 expression. (A) immortalized human LX2 hepatic stellate cells were treated with DMSO (−) (white bars), 1 μM Rosiglitazone (Ro) (grey bars), 5 μM Retinoic Acid (RA) (black bars), Ro plus RA (hatched bars), and 10−100 nM of GW501516 for 24 h before being subjected to qRT-PCR analysis of *CEACAM1* (*CC1*) mRNA levels. Data are expressed as mean ± SEM; $^*P < 0.05$ vs vehicle (−). (B) to analyze the transcriptional regulation of Ceacam1 promoter activity in LX2 cells, wild-type (nts −1100) mouse *Ceacam1* promoter and block mutants (small letters) of the PPRE (nts −557 and −551) (−ΔPPRE) site were subcloned into pGL4.10 promoterless plasmid. Luciferase activity was measured in triplicate in response to DMSO (−, white bars), retinoic acid (RA, black bars) or GW501516 (GW, vertical bars). PPREx3-TK-luc and PGL3-RARE-Luc were used as positive controls for PPRE and RXR, respectively. PGL4.10 empty vector was used as a negative control. Luciferase light units are expressed as mean ± SEM in relative light units. $^*P < 0.05$ treatment vs vehicle. (C) *CEACAM1* mRNA was evaluated in cells isolated from healthy donor tissues: quiescent HSCs (qHSCs, white bars) were sorted, plated in DMEM-FBS to be activated (aHSCs, Black bars). Microarray data were imported and CEACAM1 expression was normalized. Data are expressed as mean ± SEM; $^*P < 0.05$ vs qHSCs.

Wako, Richmond, VA), interleukin-6 (ELISA-ab178018, Abcam) and TNFα (ELISA-ab181421, Abcam) were determined per manufacturer instructions.

Cell growth was determined by MTT assay (Sigma−Aldrich) and absorbance read at 570 nm in 96-well plates. Cell growth was calculated as percent of growth in the presence of effector minus basal growth divided by maximum growth in complete medium.

2.6. Immunoprecipitation and Western blot analysis

As previously described [17], cells were Triton-lysed and subjected to SDS-PAGE followed by Western blot analysis using antibodies as listed in Supplemental data. Proteins were detected by chemiluminescence, scanned and their density normalized against tubulin (Cell Signaling) or the total amount of proteins of the signaling molecule applied on parallel gels.

For immunoprecipitation, 100 μg of protein lysates were precleared with 20 μl mixture of protein G and A sepharose beads (Invitrogen, Carlsbad, CA) at 4 °C for 2 h. Proteins were immunoprecipitated from the precleared lysates by incubation with 2 μg of their specific antibodies overnight at 4 °C, centrifuged and analyzed by SDS-PAGE and Western blot analysis.

2.7. Quantitative real-time-PCR (qRT-PCR)

Total RNA was isolated with PerfectPure RNA Tissue Kit (Fisher Scientific, Waltham, MA). cDNA was synthesized by iScript cDNA Synthesis Kit (Bio-Rad), using 1 μg of total RNA and oligodT primers (Table S1). cDNA was evaluated with qRT-PCR (StepOne Plus, Applied Biosystems, Foster City, CA), and mRNA was normalized to *GAPDH*, unless otherwise mentioned.

2.8. Statistical analysis

Data were analyzed using one-way ANOVA analysis with Bonferroni correction or two-tailed Student-t-test using GraphPad Prism 6 software. Data were presented as means ± SEM. $P < 0.05$ was considered statistically significant.

3. RESULTS

3.1. Regulation of CEACAM1 expression in human hepatic stellate cells

Rosiglitazone (Ro) elevated *CEACAM1* mRNA levels by ∼2-to-3—fold in human LX2 HSCs (Figure 1A). This likely resulted from the transcriptional activation of *Ceacam1* promoter by the binding of liganded PPARγ to the functional and well-conserved PPAR response element/retinoic acid receptor recognition site (PPRE/RXRα) between nts—557 and —543 in *Ceacam1* promoter [25]. A similar effect was exerted by retinoic acid (RA) either alone or combined with rosiglitazone (Figure 1A). As Figure 1B shows, RA induced the luciferase activity of PGL3-RARE-Luc (positive control) and of the wild-type mouse *Ceacam1* promoter (−1100pLuc) without affecting that of the empty vector (PGL4.10) [$^*P < 0.05$ vs vehicle-treated (−)]. Specifcity of the activation of RXR by RA was demonstrated by its stimulatory effect on the promoter activity of the construct harboring a mutation on the PPRE response element alone without altering RXR (−ΔPPRE). In contrast, activating PPARδ by GW501516 (100 nM) repressed CEACAM1 promoter activity (Figure 1B) and its mRNA levels (Figure 1A) in LX2 cells. Mutating the PPRE response element on *Ceacam1* promoter abolished the repressive effect of GW501516 (Figure 1B).

3.2. Loss of CEACAM1 activates human LX2 stellate cells

Activated primary human HSCs (aHSCs) exhibited lower (by >80%) CEACAM1 mRNA levels relative to quiescent cells (qHSCs) (Figure 1C). To test whether CEACAM1 loss mediated HSC activation, we examined whether lentiviral shRNA-mediated repression of CEACAM1 by >90% (Figure 2A. i and ii) could activate LX2-HSCs. Consistent with the loss of lipid content during HSC activation [26—28], knocking down CEACAM1 markedly reduced Nile red-stained fat-laden droplets relative to scrambled controls (Figure 2B.i KD vs Scr in the graphical presentation of densitometry analysis). The lost cellular fat was recovered as free glycerol in the KD-LX2 culture media (Figure 2B.ii). As predicted based on the known features of HSC activation, KD-LX2 cells exhibited lower mRNA levels of enzymes catalyzing retinyl ester (RE) synthesis [lecithin-retinol acyltransferase (LRAT)] and lipolysis [lysosomal acid lipase-LAL (LIPA), 29] (Figure 2B.iii). Reciprocally, they manifested elevated mRNA of enzymes catalyzing PUFA-triacylglycerol (PUFA-TG) synthesis [27], such as PUFA-specific fatty acid-CoA synthase 4 (ACSL4) [30], and of lipogenic genes such as SREBP-1c and fatty acid synthase (FASN), DGAT1 (the last enzyme in TG synthesis) and ATGL (TG lipase). Whether the activity of these enzymes is affected remains unclear.

Activated HSCs undergo proliferation and resist apoptosis [26,31]. Consistently, knocking down CEACAM1 markedly increased LX2 proliferation, as assessed by MTT assay (Figure 2C.i). It also led to ∼2-fold higher mRNA levels of α-smooth muscle actin (*α-SMA or ACTA2*) and *COL1α1*, markers of mesenchymal cell activation (myofibroblastic transformation) [26] (Figure 2C.ii). The latter could result from increased activation of TGFβ canonical signaling pathway, as assessed by Western blot analysis of phosphorylated Smad2/3 (Figure 2D). This demonstrated that CEACAM1 loss activated KD-LX2 cells.

3.3. Delineating the mechanism underlying LX2 activation by CEACAM1 deletion

Following phosphorylation by epidermal growth factor (EGFR) and insulin (IR) receptors, CEACAM1 sequesters Shc and reduces its coupling to the receptors to suppress downstream Shc/MAPK-mediated cell growth and proliferation pathways [32,33]. Consistently, insulin (100 nM) treatment for 5 min stimulated IRβ and MAPK phosphorylation in both groups of cells (Figs. S2B—C, + vs — insulin), and induced their proliferation, as assessed by MTT assay (Fig. S2D, + vs — insulin). In the absence of insulin, KD-LX2 cells manifested a higher basal phosphorylation of MAPK, but not IRβ (Figs. S2B—C), in parallel to higher cell growth relative to their Scr-LX2 controls (Fig. S2D). This implicated an IR-independent pathway in KD-LX2 basal activation.

We then examined whether the FAs released from KD-LX2 cells (Figure 3A.i, black vs white bar)], could stimulate EGFR pathways [33] to activate HSCs [34]. As Figure 3B.i shows, incubating Src-LX2 in the conditioned media of KD-LX2 cells (Scr/Cond) markedly reduced *CEACAM1* (*CC1*) mRNA levels (∼75%) (grey vs white bar; $P < 0.05$). This likely resulted from increased *PPARβ/δ* expression (Figure 3B.ii) and its activation by the released FAs. Consistently, blocking lipolysis by nicotinic acid (NA) normalized FA levels in KD-LX2 media (Figure 3A.i, diagonally-hatched vs white and vertically-hatched bars) and subsequently, restored *CEACAM1* mRNA levels in Scr/Cond (Figure 3B.i, horizontally-hatched vs vertically-hatched bar).

Western blot analysis revealed higher EGFR phosphorylation in KD and Src/Cond cells in the absence of NA (Figure 3C.i, — lanes 1 and 5 vs lane 3), but not in its presence (Figure 3C.i, + vs — lanes/cell group). This demonstrated that EGFR was activated in response to FA-containing conditioned media. Consistent with reduced CEACAM1 level, CEACAM1/Shc binding was lower in Scr/Cond than Scr cells, as demonstrated by its repressed detection in the Shc immunopellet (Figure 3C.ii, — lane 5 in Scr/Cond vs — lane 3 in Scr). This led to a reciprocal recovery of Shc in the EGFR immunopellet of Scr/Cond relative to Scr cells (Figure 3C.iii, — lane 5 in Scr/Cond vs — lane 3 in Scr), and activation of downstream MAPK pathways (Figure 3C.iv, — lane 5 in Scr/Cond vs — lane 3 in Scr) and NF-κB (Figure 3C.v, — lane 5 in Scr/Cond vs — lane 3 in Scr). This induced cell proliferation, as assessed by elevated PCNA protein levels (Figure 3C.vi, — lane 5 in Scr/Cond vs — lane 3 in Scr) and MTT assay (Figure 3B.v, grey vs white bar). Additionally, *PPARγ1* mRNA levels were lowered in Scr/Cond-LX2 cells (Figure 3B.iii, grey vs white bar), as expected during HSC activation and in contrast to the rise in *PPARβ/δ* levels [35], which was likely activated by the excess FAs produced in KD-LX2 and Src/Cond-LX2 cells (Table S2). Consistent with increased myofibroblastic transformation, *ACTA2* mRNA levels were induced by ∼two-to-threefold in KD and Scr/Cond LX2 cells (Figure 3B.iv, grey and black vs white bar). Reversal of these processes in Scr/Cond cells by NA treatment (+ vs — lanes in Scr/Cond) further supported a role for FAs

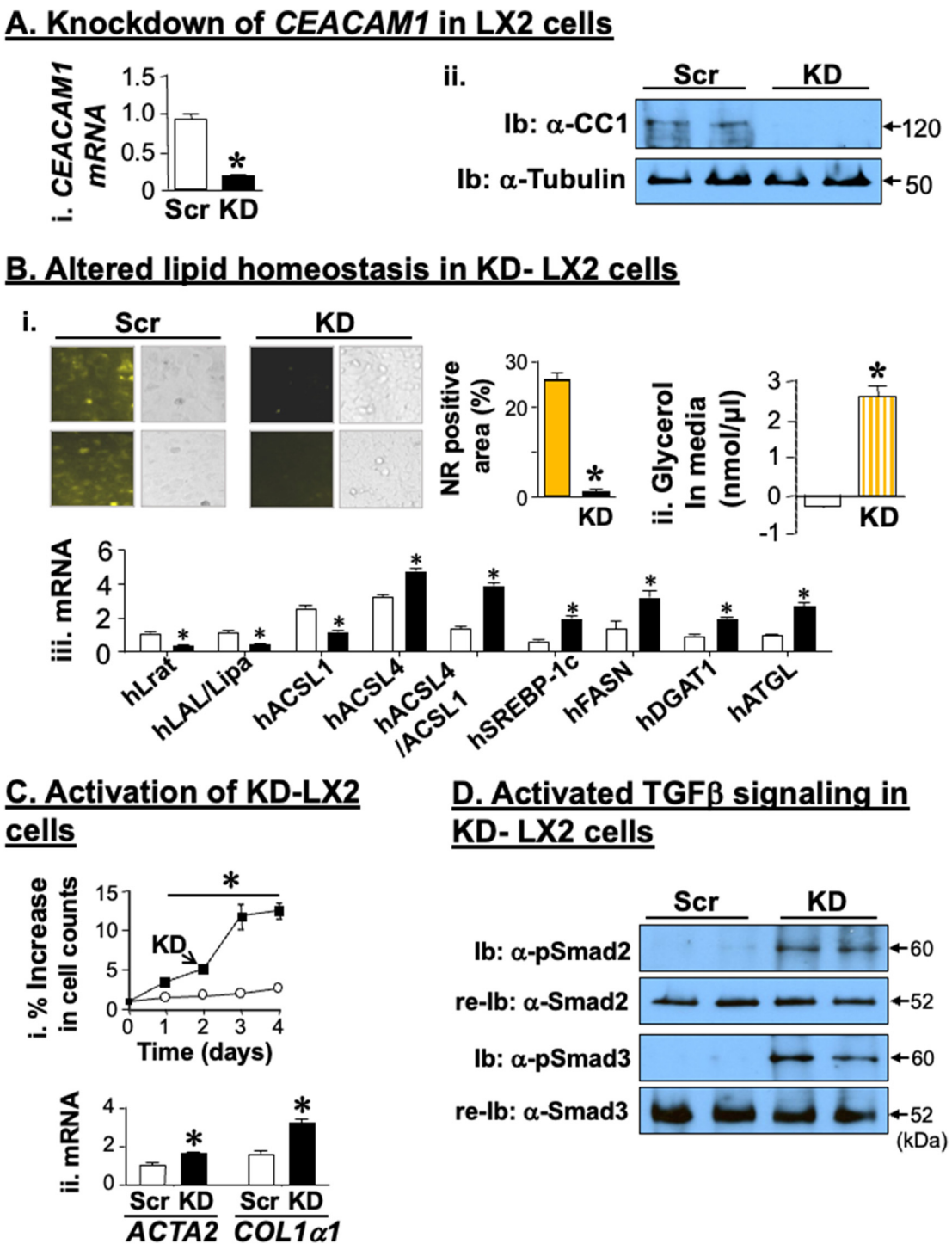

Figure 2: Activation of LX2 human hepatic stellate cells by CEACAM1 deletion. (A) LX2 cells were subjected to shRNA-mediated knockdown of *CEACAM1* (KD) and (i) analyzed by qRT-PCR in triplicate to assess the decrease in *CEACAM1* mRNA in KD-LX2 (black bars) vs Scr-LX2 scrambled control cells (white bars). mRNA was normalized to *GAPDH* mRNA and data represented as mean ± SEM; $^*P < 0.05$ vs Scr-LX2; (ii) CEACAM1 protein levels were assessed by immunoblotting (Ib) the upper half of the membrane with α-CEACAM1 (α-CC1) antibody and the lower half with α-tubulin to normalize per loaded proteins. (B) to examine lipid metabolism, (i) cells were grown in at least 3 plates/stable line, stained with Nile Red to depict fat (yellow) droplets. Positive fat stains were evaluated by densitometry, presented as % area graphically as mean ± SEM; $^*P < 0.05$ vs Scr-LX2; (ii) free glycerol level was assayed in the media of the stained cells as a measure of lipolysis. Experiments were done in triplicate. Data are expressed as mean ± SEM; $^*P < 0.05$ vs Scr-LX2; (iii) qRT-PCR mRNA analysis of genes implicated in lipid metabolism was performed in triplicate. Values are expressed as mean ± SEM. $^*P < 0.05$ vs Scr-LX2. (C) to assess LX2 activation, (i) KD-LX2 and Scr-LX2 cells were subjected to MTT assay in triplicate. Data represent mean ± SEM; $^*P < 0.05$ vs Scr-LX2; (ii) qRT-PCR analysis was performed in triplicate to assess *ACTA2* and *COL1α1* mRNA levels as markers of fibrogenic activity. Data represent mean ± SEM; $^*P < 0.05$ vs Scr-LX2. (D) to examine TGFβ signaling, cell lysates were immunoblotted with α-phosphoSmad2 or α-phosphoSmad3 antibody (α-pSmad) followed by re-immunoblotting (re-Ib) with α-Smad 2 or α-Smad 3 antibodies, respectively, for normalization.

release from activated KD-LX2 in the autocrine activation of EGFR-Shc-MAPK to increase HSCs proliferation.

Interleukin-6 (IL-6), a transcriptional target of NF-κB, was also elevated in KD media (Figure 3Aii, black vs white bar). Consistent with the anti-inflammatory effect of NA [36] and its inhibition of IL-6 production [37], NA treatment reversed IL-6 level in KD media (Figure 3Aii, + vs − lane) without affecting that of TNFα (Figure 3Aiii, + vs − lane). Because IL-6 transactivates EGFR [38], we then tested whether the rise in IL-6 contributed to EGFR basal activation in KD-LX2 and Scr/Cond-LX2 cells. To this aim, we carried out media transfer experiments in the absence and presence of Gefitinib, an EGFR tyrosine kinase inhibitor [23]. As Fig. S3A shows, Gefitinib inhibited EGFR phosphorylation in KD-LX2 and Scr/Cond-LX2 cells (+ vs − lanes). In parallel, it reduced *PPARβ/δ* (Fig. S3B) and reciprocally induced *PPARγ1* mRNA levels in these cells (Fig. S3C, horizontally-hatched vs grey bar in Scr/Cond-LX2 and diagonally-hatched vs black bar in KD-LX2 cells) to stimulate their *CEACAM1* mRNA levels (Fig. S3D). This was associated with the ability of Gefitinib to prevent Scr/Cond-LX2 activation, as demonstrated by reduction and normalization of *ACTA2* mRNA levels (Fig. S3E) and their cell proliferation (Fig. S3F, + vs − lanes).

3.4. Activation of primary HSCs from *Cc1*$^{-/-}$ null mice

In support of HSCs activation when their CEACAM1 is absent, primary HSCs from global *Cc1*$^{-/-}$ nulls exhibited higher mRNA levels of *Pparβ/δ*, *Pcna*, and *Acta2* than HSCs from wild-type mice (Table S3). They also exhibited higher *Srebp-1c* and *Fasn* mRNA levels. Moreover, their media induced the mRNA levels of these genes in wild-type HSCs (Table S3). NA treatment normalized these parameters in HSCs from *Cc1*$^{-/-}$ and *Cc1*$^{+/+}$*/Cond* cells (Table S3). This proposed that CEACAM1 loss in HSCs activated them and caused their myofibroblastic transformation to contribute to hepatic fibrosis in *Cc1*$^{-/-}$ nulls [14].

3.5. *LratCre* + *Cc1*$^{fl/fl}$ mice with conditional deletion of *Ceacam1* in HSCs are insulin sensitive

Because *Ceacam1* loss in endothelial cells and hepatocytes could also contribute to hepatic fibrosis in *Cc1*$^{-/-}$ nulls [14], we then assessed the effect of deleting *Ceacam1* exclusively from HSCs on hepatic fibrosis. To this end, we generated *LratCre* + *Cc1*$^{fl/fl}$ mice with conditional deletion of *Ceacam1* in HSCs, as demonstrated by their intact *Ceacam1* expression in bone marrow macrophages, hepatocytes and liver endothelial cells (Figure 4A). Triple immunofluorescence stain of liver tissue sections showed specific deletion of CEACAM1 (Red) in Desmin^{+} stellate cells in *LratCre* + *Cc1*$^{fl/fl}$ mice but not in their control mice or in other cells (such as ATP1A1^{+}/ABCB11^{+} hepatocytes or CD31^{+} endothelial cells) where CEACAM1 expression was intact (Fig. S4). These mice exhibited normal body weight, visceral fat mass, plasma NEFA and triacylglycerol levels (Table 1). *LratCre* + *Cc1*$^{fl/fl}$

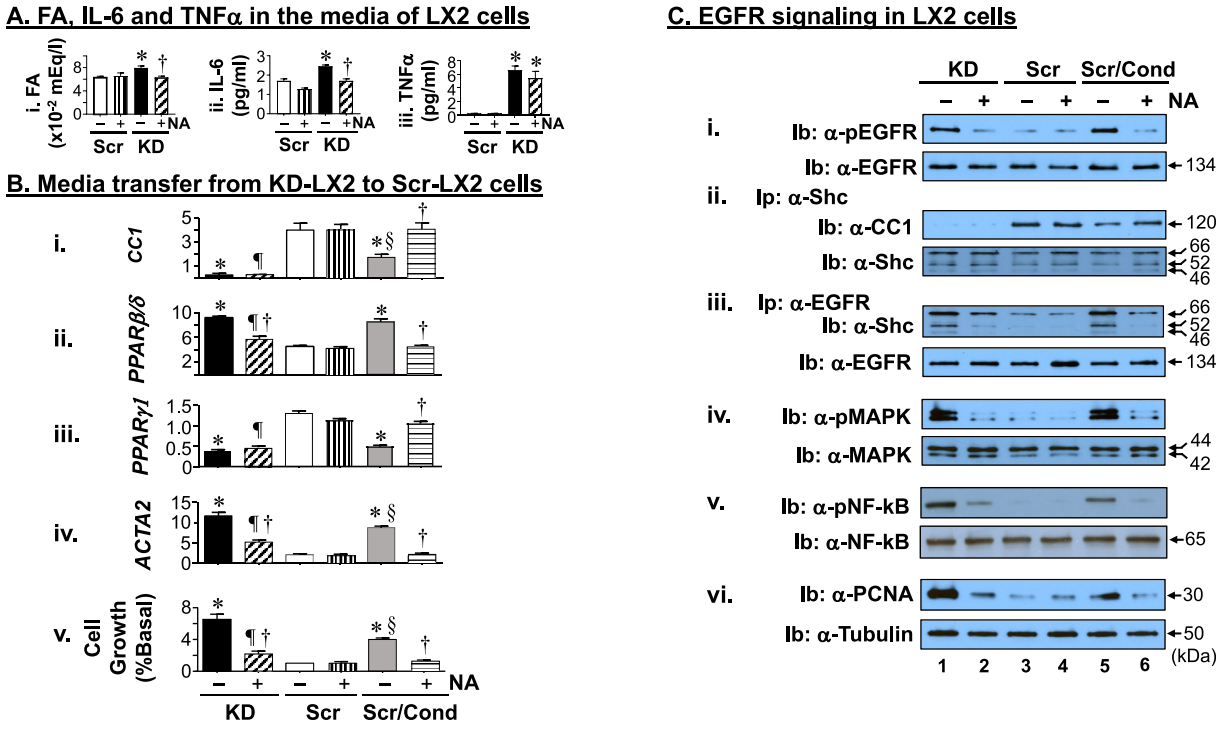

Figure 3: Scr-LX2 activation by conditioned media from KD-LX2 cells. Src-LX2 and KD-LX2 cells were incubated with nicotinic acid (NA) (+) or with vehicle (−) for 24 h before (A) media were collected to assay levels of fatty acids (i), IL-6 (ii) and TNFα (iii). Data represent mean ± SEM; $^{*}P < 0.05$, KD-LX2 vs Scr-LX2 cells/treatment type; $^{\dagger}p < 0.05$, NA-treated vs untreated/cell group. (B) media of KD-LX2 cells (conditioned media) were transferred to pre-washed Scr group (Scr/Cond) before cells were harvested for qRT-PCR analysis of the mRNA of *CC1*, *PPARβ/δ, PPARγ1 and ACTA2* (Figure 3B.i-iv) and cell growth by MTT assay in triplicate and repeated twice (Figure 2B.v). $^{*}P < 0.05$ untreated KD and Scr/Cond vs untreated Scr-LX2 cells; $^{\dagger}P < 0.05$ NA-treated vs untreated/cell group; $^{\S}P < 0.05$ untreated Scr/Cond vs untreated KD, and $^{\P}P < 0.05$ NA-treated KD vs NA-treated Scr and NA-treated Scr/Cond cells. The latter indicates that although NA treatment decreased the mRNA of *PPARβ/δ* and *ACTA2* as well as cell growth, it did not completely restore their values to those in Scr-LX2 controls, as it did in Scr/Cond cells. This is likely due to persistent absence of CEACAM1 (and low *PPARγ1*) with sustained TNFα (iii) levels in these donor KD-LX2 cells. (C) Western blot analysis of EGFR signaling in cells described above: liver lysates were subjected to immunoblotting (Ib) with antibodies against (i) phospho-EGFR (α-pEGFR), (iv) phospho-MAPK (α-pMAPK), (v) phospho-NF-kB (α-pNF-kB), and (vi) α-PCNA and in parallel gels, with their specific antibodies for normalization. (ii) some lysates were subjected to immunoprecipitation (Ip) with Shc antibody followed by immunoblotting (Ib) with antibodies against CEACAM1 (α-CC1) and Shc (α-Shc). (iii) Lysates were subjected to immunoprecipitation (Ip) with α-pEGFR antibody followed by immunoblotting (Ib) with α-Shc and α-EGFR antibodies. Gels represent two separate experiments. The apparent molecular mass (kDa) is indicated at the right hand-side of each gel.

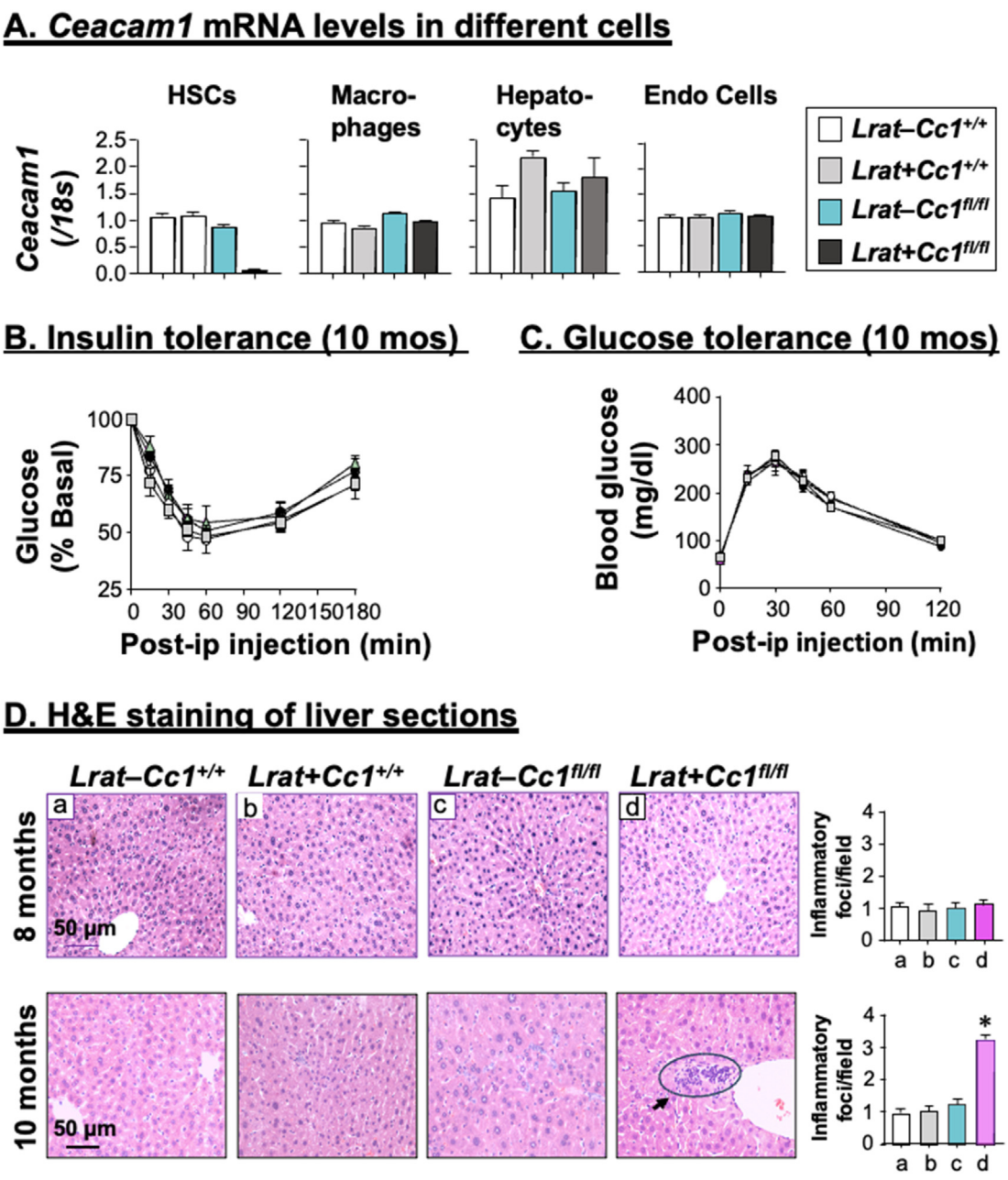

Figure 4: Metabolic phenotyping of *LratCre* + *Cc1*$^{fl/fl}$ mice. (A) Primary cells were isolated from male mutants and their littermate controls (n = 2 mice/genotype) at 2–4 months of age except for HSCs which were isolated from mice at 8 months of age (n = 5/genotype). *Ceacam1* mRNA levels were analyzed by qRT-PCR in triplicate and normalized to *18s*. Values are expressed as mean ± SEM. (B–C) 10-month-old male mice (n ≥ 7–8/genotype) were injected intraperitoneally with insulin or glucose to assess glucose disposal in response to insulin (B) and glucose (C). Values were expressed as mean ± SEM. (D) Livers were removed from 8- and 10-month-old *Lrat* + *Cc*$^{1fl/fl}$ male mice and their 3 littermate controls (n = 4–5/genotype), sectioned and stained with H&E staining to identify foci of inflammatory cell infiltrates in mutants (panel d) and their littermate controls (panels a–c). Values are expressed as mean ± SEM in the accompanying inflammatory foci quantification graph. *$P < 0.05$ mutants vs the 3 littermate controls.

mice exhibited normal hepatic insulin clearance (steady-state C-peptide/insulin molar ratio) and normo-insulinemia relative to their control counterparts (Table 1). They also showed normal tolerance to exogenous glucose and insulin (Figure 4B,C, respectively), with normal fasting and fed blood glucose levels (Table 1). Consistent with normo-insulinemia, hepatic triacylglycerol levels were normal (Table 1) and H&E stain did not detect lipid droplet deposition in liver sections (Figure 4D.d). Moreover, the mRNA levels of genes involved in fatty acid transport (CD36 translocase) and lipogenesis [Srebp-1c, and fatty acid synthase (Fasn)] were normal (Table S4). Together, this demonstrated that conditional *Ceacam1* deletion from HSCs did not cause insulin resistance or hepatic steatosis, consistent with intact expression of CEACAM1 in hepatocytes.

3.6. Increased inflammation in *LratCre* + *Cc1*$^{fl/fl}$ livers

H&E staining indicated diffused mononuclear inflammatory foci in the liver parenchyma of *LratCre* + *Cc1*$^{fl/fl}$ mutants without ballooning or altered hepatocellular architecture starting at 10 months of age, as shown by the lack of inflammatory foci at 8 months of age [Figure 4D.d (and graph)].

Table 1 — Plasma and tissue biochemistry in mice at 10 months of age.

	LratCre—Cc1$^{+/+}$	*LratCre* + *Cc1*$^{+/+}$	*LratCre—Cc1*$^{fl/fl}$	*LratCre* + *Cc1*$^{fl/fl}$
Body weight (g)	29.4 ± 2.2	26.7 ± 1.2	28.3 ± 1.7	28.5 ± 1.1
% WAT/BW	1.9 ± 0.9	1.6 ± 0.5	1.2 ± 0.4	1.2 ± 0.3
NEFA (mEq/l)	0.5 ± 0.1	0.6 ± 0.1	0.4 ± 0.1	0.5 ± 0.1
TG (mg/dl)	48.4 ± 8.9	50.4 ± 6.5	42.8 ± 13.2	43.4 ± 7.0
Insulin (pM)	80.5 ± 10.7	74.7 ± 4.7	73.7 ± 2.1	78.5 ± 7.0
C-peptide (pM)	198.6 ± 36.4	193.1 ± 36.7	177.9 ± 22.6	219.4 ± 45.6
C/I molar ratio	2.3 ± 0.3	2.6 ± 0.3	2.4 ± 0.3	2.9 ± 0.7
Fast Glucose (mg/dl)	67. ± 9.	60. ± 6.	71. ± 6.	64. ± 5.
Fed Glucose (mg/dl)	116. ± 7.	118. ± 4.	112. ± 6.	116. ± 9.
Hepatic TG (μg/mg)	58.7 ± 8.7	65.5 ± 9.2	59.1 ± 9.9	58.7 ± 15.2

Blood was drawn from male mice (10 months of age, n ≥ 5/genotype) at 2100 h to assess fed glucose levels. Following a recovery period of 3 days, mice were fasted overnight before blood was drawn and tissues were excised at 1100 h in the next morning. Except of blood glucose levels, other values refer to plasma levels, unless otherwise mentioned. Hepatic TG is measured as μg/mg protein. Values are expressed as mean ± SEM. BW: Body weight; WAT: white adipose tissue; %WAT/BW: visceral obesity; C/I: Steady-state C-peptide/Insulin molar ratio as a measure of hepatic insulin clearance; NEFA: Non-esterified fatty acid; TG: Triacylglycerol.

Immunohistochemical (IHC) analysis revealed an increase in macrophage recruitment (CD68) and activation (Mac2) [Figure 5A.i-ii (and graphs), panels d vs a-c, respectively]. It also showed elevated immunostained myeloperoxidase (MPO) levels [Figure 5A.iii (and graph), panel d vs a-c], which together with increased mRNA of MPO and elastase (Table S4), demonstrated an increase in neutrophil accumulation in the liver parenchyma of mutant livers. In addition to MPO, a granulocyte-specific transcription factor (STAT3) was activated (phosphorylated) at 10 months (Figure 5B), but not at 8 months of age (Fig. S5A). This likely resulted from the ~2-to-3-fold concomitant rise in hepatic IL-6 mRNA levels (Figure 5C vs Fig. S5B) and in the plasma levels of this pro-inflammatory cytokine (Figure 5D).

Consistent with IL-6 as a transcriptional target of NF-κB, the p65(NF-κB) subunit was basally activated (phosphorylated) in the livers of 10-month-old (Figure 5B), but not 8-month-old (Fig. S5A) *LratCre* + *Cc1*$^{fl/fl}$ mutants. This likely resulted from reduced Shc sequestration in the absence of CEACAM1 and the reciprocal increase in its coupling to EGFR [33]. In addition to IL-6, activated p65(NF-κB) could induce Mcp-

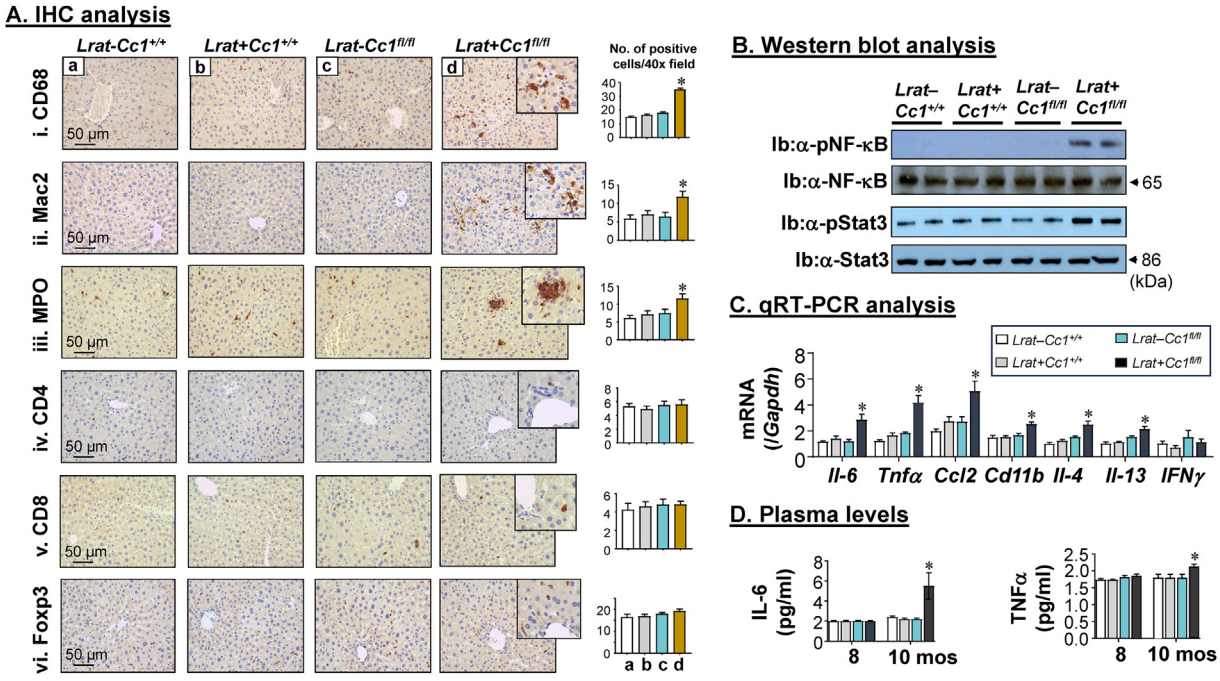

Figure 5: Increased inflammation in *LratCre* + *Cc1*$^{fl/fl}$ livers. (A) livers were removed from 10-month-old *LratCre* + *Cc1*$^{fl/fl}$ mutants and their three controls (n = 4—5 mice/genotype) and subjected to (A) immunohistochemical (IHC) analysis with: (i) CD68 to assess macrophage recruitment, (ii) Mac-2 to examine macrophage activation, (iii) MPO to evaluate neutrophil accumulation, CD4 (iv) and CD8 (v) to immunostain T cells and (vi) Foxp3 to determine the anti-inflammatory Treg pool. Representative images taken at 50 μm magnification are shown with insets at 20 μm. Values are expressed as mean ± SEM in the accompanying quantification graph. $^*P < 0.05$ mutants (d) vs the 3 littermate controls (a—c). (B) liver lysates were subjected to immunoblotting (Ib) with antibodies against the phosphorylated p65 subunit of NF-κB (α-pNF-kB), and α-pStat3. To normalize against added proteins, gels were analyzed by SDS gel electrophoresis in parallel and proteins immunoblotted with specific antibodies. Representative gels include 2 different mice/genotype. (C) liver lysates (n = 6/each genotype) were analyzed in duplicate by qRT-PCR using gene-specific primers and normalized to *Gapdh*. Values are expressed as mean ± SEM. $^*P < 0.05$ vs all three controls. (D) Male mice (8 and 10 months of age, n ≥ 6/genotype/age group) were fasted overnight before blood was drawn at 1100 in the next morning and their plasma IL-6 and TNFα levels were analyzed. Values are expressed as mean ± SEM. $^*P < 0.05$ vs all three controls.

1/Ccl2 transcription [39], as shown in Figure 5C, to recruit monocytes/macrophages into active inflammatory foci in mutant livers. Together with IL-6, Ccl2 could induce CD11b+ macrophage pool (Figure 5C) and its differentiation toward the M2 type [40,41], which is partly mediated by elevated levels of IL-4/IL-13 type 2 cytokines (Figure 5C). Together with no increase in the mRNA levels of Th1-derived cytokine IFNγ (Figure 5C) or in plasma TNFα levels (Figure 5D), this points to the mounting of an M2 response in mutant livers, mediated partly by sustained IL-6/STAT3 phosphorylation [42]. In contrast to macrophages, IHC (Figure 5A.iv-v) and qRT-PCR (Table S4) analyses revealed no significant increase in pro-inflammatory CD4+T and CD8+T lymphocytes. Moreover, there was no increase in the anti-inflammatory Treg immunostain (Foxp3) (Figure 5A.vi), or in hepatic IL-10 expression (Table S4). Thus, liver injury in *LratCre* + *Cc1*$^{fl/fl}$ mice was associated with a Th2 response marked by elevated IL-4/IL-13 secretion by hepatic lymphocytes that could activate infiltrated myeloid cells (macrophages and neutrophils) to induce their M2 genes expression.

3.7. Spontaneous fibrosis in *LratCre* + *Cc1*$^{fl/fl}$ livers

Because activated hepatic macrophages could initiate and maintain the myofibroblastic transformation of HSCs [41], we then tested whether *LratCre* + *Cc1*$^{fl/fl}$ mice developed hepatic fibrosis. Based on Sirius Red staining, *LratCre* + *Cc1*$^{fl/fl}$, but not their controls, developed an extensive interstitial chicken-wire pattern of collagen deposition starting at 10 months of age (Figure 6A.d vs a-c, and vs Fig. S6A.d at 8 months). Consistently, the mRNA levels of pro-fibrogenic genes (*Acta2*, *Col1α1*, *Col3α1*, and *Tgfβ*) were induced in the livers of 10-month-old (Figure 6B.i), but not 8-month-old (Fig. S6B) mutants. Hepatic fibrosis could be mediated by the activation of the canonical TGFβ—SMAD2/3 profibrogenic pathway, as demonstrated by SMAD2 phosphorylation (Figure 6C) with no change in the expression of its inhibitor, Smad7 (Figure 6B) at 10 months but not at 8 months of age (Fig. S6C).

Activated HSCs modulate the extracellular matrix (ECM) composition, mediated by MAPK, NF-κB and TGFβ-SMAD2/3 pathways. This involves the regulation of the expression of the matrix metalloproteinases (MMPs) and the tissue inhibitor of metalloproteinases (TIMPs) that are implicated in the production as well as the resolution of excess collagen and other ECM components. Consistently, 10-month-old *LratCre* + *Cc1*$^{fl/fl}$ livers displayed higher mRNA (Figure 6B.i) and protein levels (Figure 6C) of MMP9, MMP13 and TIMP1 relative to controls. They also exhibited a ∼2-fold increase in the mRNA levels of hepatic *Mmp 2*, *Timp 2* and *Timp 3* (Figure 6B.i). Whereas MMP9, TIMP1 and TIMP2 are pro-fibrogenic, MMP2 and TIMP3 block fibroblastic activation and increase collagen clearance [43]. MMP13 can promote collagen production as well as its clearance [43].

Coupled with oxidative stress, TGFβ signaling could cause hepatocellular injury [44]. Consistently, mutant livers manifested higher mRNA levels of genes implicated in oxidative stress (*Nox1* and *Nox4*) (Table S4) and hepatocytes injury (*Txn*, *Nqo*, *Nrf1* and *Hgf*) (Figure 6B.ii). This could drive liver dysfunction, as determined by higher plasma alanine transaminase (ALT) and aspartate aminotransferase (AST) content in 10-month-old but not 8-month-old mutants as compared to control mice (Figure 6D).

3.8. Conditioned media from *LratCre* + *Cc1*$^{fl/fl}$ HSCs activates wild-type HSCs via an EGFR-mediated mechanism

As above, NA treatment blocked the release of FAs (Figure 7A. i, + vs − lane) and IL-6 (Figure 7A.ii, + vs − lane) into the media of *LratCre* + *Cc1*$^{fl/fl}$ HSCs (KO). Thus, we next examined whether media from KO—HSCs (Cond) could activate wild-type (WT) HSCs and whether this could be blocked by NA treatment. As Figure 7B.i shows, incubating WT-HSCs with media from KO HSCs (WT/Cond) repressed *Ceacam1* expression by ∼65% relative to WT-HSCs incubated in regular culture media (− lanes, grey vs white bar). This likely resulted from increased *Pparβ/δ* and reduced *Pparγ 1* expression (Figure 7B.ii-iii, respectively, − lanes, grey vs white bars).

This reciprocal change in *Pparβ/δ* and *Pparγ 1* expression, together with higher expression of *Acta2* (Figure 7B.iv) and *Pcna* (Figure 7B.v) in WT/Cond than WT cells in regular media (grey vs white bars) demonstrated a higher myofibroblastic activation and proliferation of WT/Cond than WT cells. Furthermore, NA treatment reversed these changes in *Pparβ/δ*, *Pparγ 1*, *Acta2* and *Pcna* mRNA levels in parallel to restoring *Ceacam1* expression in WT/Cond (Figure 7B.i-vi, + vs − bars, horizontally-hatched vs vertically-hatched bars). Gefitinib had a similar effect on the mRNA of these genes in WT/Cond (Figure 7B.vii-x, + vs − bars, horizontally-hatched vs vertically-hatched bars).

Table S5 shows that KO—HSCs exhibited 2-to-4—fold reduction in the mRNA levels of *Lrat* and *Lal/Lipa*, with a reciprocal ∼12-fold increase in *Acsl4/Acsl1* and an ∼4-to-6—fold increase in the mRNA levels of *Dgat1* and *Atgl*. It is likely that the increase in FAs release activated PPARβ/δ to reduce *Ceacam1* expression in WT/Cond cells. This would lower Shc sequestration and elevate its reciprocal coupling with EGFR to activate downstream pro-fibrogenic and proliferation pathways (increased *Acta2* and *Pcna*, respectively). Reversal of these changes in lipid metabolism in WT/Conds by Gefitinib further demonstrated that EGFR activation mediated the myofibroblastic transformation of HSCs by *Ceacam1* loss.

3.9. Conditioned media from young *LratCre* + *Cc1*$^{fl/fl}$ HSCs activates wild-type HSCs

To further investigate whether deleting *Ceacam1* can cell-autonomously activate HSCs before other liver cells could be injured, we examined whether media from KO—HSCs derived from 4 month-old mice could activate WT-HSCs. As Figure 8Ai shows, KO—HSCs from young mice released ∼2-fold higher FAs than their WT counterparts. Incubating the latter with KO conditioned media stimulated their FA release. In contrast, IL-6 levels was significantly lower in these young KO—HSCs relative to WT-HSCs which released less IL-6 upon their incubation with the conditioned media (Figure 8Aii). The higher FA in these young KO—HSCs did not affect *PPARβ/δ* mRNA levels, but could have activated them, as demonstrated by their significantly lower *Ceacam1* mRNA levels relative to WT (Figure 8B), which could also result from their lower *PPARγ 1* mRNA levels. Nevertheless, incubating WT-HSCs in the media of young KO—HSCs yielded a remarkable decrease in *Ceacam1* levels (WT/Cond) in parallel to elevated FA and low IL-6 levels in the conditioned media (Figure 8B). Consistent with HSC activation, mRNA levels of *Acta2* and *Col1α1* were elevated in WT/Cond cells (Figure 8B). Thus, HSCs devoid of *Ceacam1* bears an intrinsic ability to cause stellate cell activation independently of other liver cell types.

4. DISCUSSION

The current study demonstrated that CEACAM1's expression in cultured human LX2-HSCs is supported by autocrine PPARγ and retinoic acid transcriptional upregulation, and that activation of primary human HSCs significantly repressed CEACAM1 expression. On the other hand, loss of CEACAM1 in LX2 and primary murine HSCs activated them. This was manifested by reduced PPARγ$_1$ and retinoic acid levels with reciprocal elevation in PPARβ/δ and PUFA-TG content,

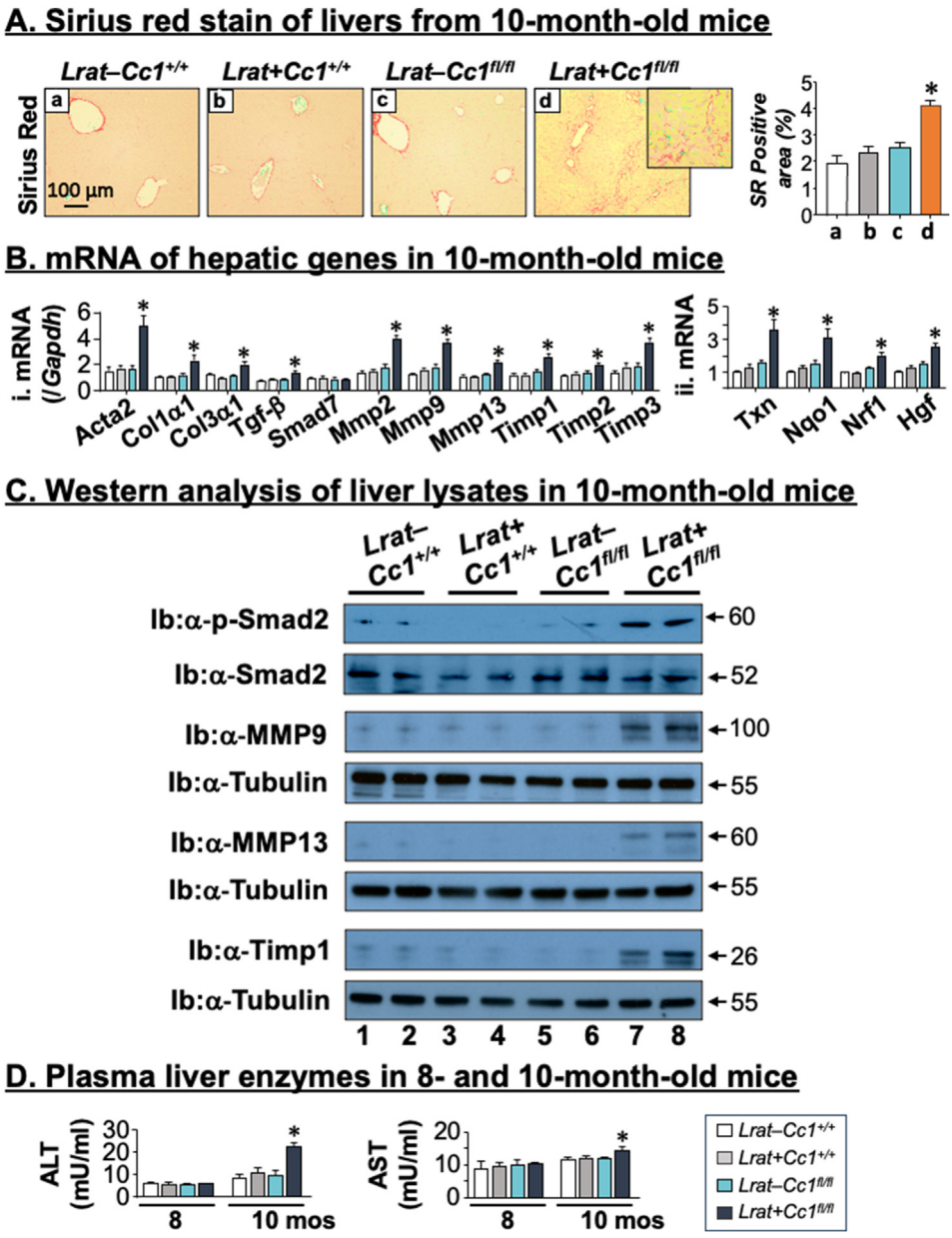

Figure 6: Spontaneous hepatic fibrosis in *LratCre* + *Cc1*$^{fl/fl}$ mice. Livers were removed from 10-month-old *LratCre*+ *Cc1*$^{fl/fl}$ male mice and their 3 littermate controls (n = 4–5/genotype). (A) Sirius red staining revealed increased deposition of interstitial chicken-wire pattern of collagen fibers in mutants (panel d) vs their littermate controls (panels a–c). Values are expressed as mean ± SEM in the accompanying quantification graph. *$P < 0.05$ mutants vs the 3 littermate controls. (B) liver lysates (n = 6/each genotype) were analyzed in duplicate by qRT-PCR using gene-specific primers and normalized to *Gapdh* to assess mRNA levels of genes involved in inflammation (i) and in hepatocytes injury (ii). Values are expressed as mean ± SEM. *$P < 0.05$ vs all three controls. (C) Western Blot analysis of liver lysates from *LratCre* + *Cc1*$^{fl/fl}$ male mice (lanes 7–8) and their *LratCre* – *Cc1*$^{+/+}$ (lanes 1–2), *LratCre* + *Cc1*$^{+/+}$ (lanes 3–4) and *LratCre* – *Cc1*$^{fl/fl}$ (lanes 5–6) controls. Phosphorylated Smad2 (α-pSmad2) normalized against α-Smad2. The protein levels of α-MMP9, α-MMP13 and α-Timp1 were normalized against α-Tubulin. Gels represent two different mice/genotype. The apparent molecular mass (kDa) is indicated at the right hand-side of each gel. (D) Male mice (8 and 10 months of age, n ≥ 6/genotype/age group) were fasted overnight before blood was drawn at 1100 in the next morning and their plasma ALT and AST levels were analyzed. Values are expressed as mean ± SEM. *$P < 0.05$ vs all three controls.

respectively. Because CEACAM1 inhibits FASN activity under normoinsulinemic conditions [45], suppressing *Ceacam1* transcription by PPARβ/δ [25] (and by the loss of PPARγ), likely mediated the increase in TG synthesis in mutant HSCs. In light of the anti-lipogenic and anti-fibrogenic effect of FASN inhibitors [46], the current data propose a key role for HSCs' CEACAM1 in preventing hepatic fibrosis.

CEACAM1 expression is highest in hepatocytes. Its deletion in these cells impaired hepatic insulin clearance to cause hyperinsulinemia-driven insulin resistance, *de novo* lipogenesis and inflammation [15]. It also caused hepatic fibrosis, whereas hepatocytes-specific rescuing of CEACAM1 reversed steatosis and fibrosis in parallel to restoring insulin sensitivity in *Cc1*$^{-/-}$ null mice. This points to a key role for hyperinsulinemia-driven steatosis in hepatic fibrosis caused by CEACAM1 loss in hepatocytes [31]. In contrast, *Ceacam1* deletion from endothelial cells caused hepatic fibrosis in the absence of insulin resistance and hepatic steatosis [17]. The phenotype was driven by

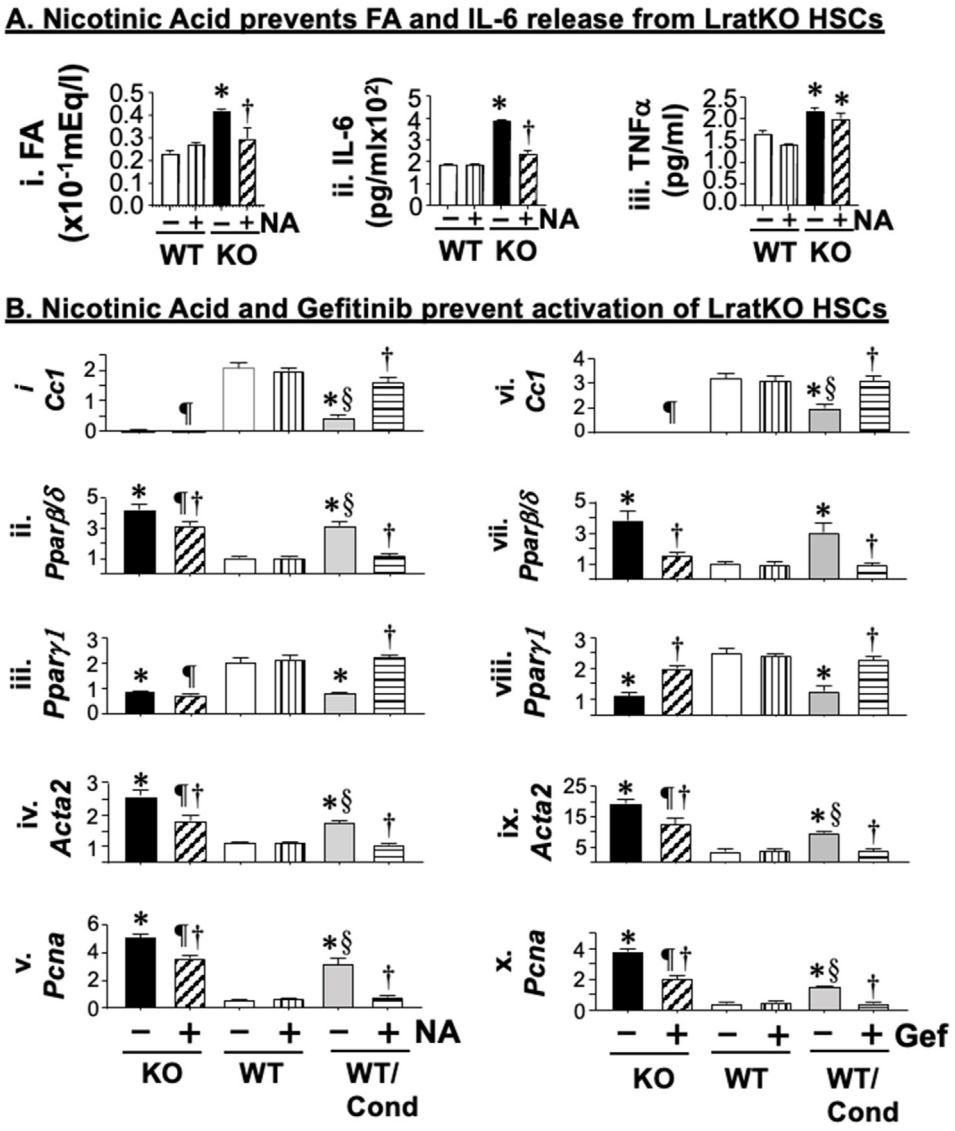

Figure 7: EGFR-mediated activation of *LratCre* + *Cc1*$^{fl/fl}$ HSCs. Primary HSCs were isolated from ≥8 *LratCre* + *Cc1*$^{fl/fl}$ mice (KO) and a combination of wild-type (*LratCre* − *Cc1*$^{+/+}$, *LratCre* + *Cc1*$^{+/+}$ and *LratCre* − *Cc1*$^{fl/fl}$) mice (WT); all at ≥8 months of age. Cells were treated with (+) or without (−) NA and the media were collected and combined to assess (A) FA (i), IL-6 (ii) and TNFα (iii) levels. Values are mean ± SEM. $^{*}P < 0.05$ KO (−) vs WT (−); $^{\dagger}P < 0.05$ NA-treated vs untreated/mouse group. (B) the conditioned KO media was transferred to WT HSCs (WT/Cond) for 24 h, while a parallel set of WT-HSCs was incubated in regular culture media and the mRNA levels were analyzed by qRT-PCR analysis. In some experiments, conditioned media without NA were transferred to WT-HSCs and the cells were treated with or without Gefinitib (vi-x). Cells were harvested for qRT-PCR analysis in triplicate of the mRNA levels relative to *Gapdh*. Values are expressed as mean ± SEM; $^{*}P < 0.05$ untreated KO and WTCond vs WT in regular media; $^{\dagger}P < 0.05$ treated vs untreated/cell group; $^{\S}P < 0.05$ untreated WT/Cond vs untreated KO in regular media, and $^{\P}P < 0.05$ treated KO vs treated WT in regular media and treated WT/Cond cells.

hyperactivation of the vascular endothelial growth factor (VEGFR)/NF-κB pathway and increased synthesis of endothelin1 and of its pro-fibrogenic signals via its receptor A in HSCs. Inflammation in this endothelial cell mutant preceded hepatic fibrosis and implicated macrophage activation in addition to mounting a Th1 response by T lymphocytes.

Like its deletion from endothelial cells, conditional deletion of *Ceacam1* from HSCs caused hepatic fibrosis in the absence of insulin resistance and hepatic steatosis. However, it occurred concurrently to inflammation and was mediated by activation of EGFR by FA and IL-6, a transcriptional target of NF-kB. Sustained activation of the IL-6/STAT3 pathway could mediate the mounting of a Th2/M2 response in *LratCre* + *Cc1*$^{fl/fl}$ livers, as in *Stat1* nulls that exhibited activation of the M2 macrophage pool without a significant increase in pro-inflammatory T lymphocytes [47].

In addition to EGFR/NF-κB pathway, the EGFR/MAPK proliferative pathway was also activated in KD-LX2 HSCs devoid of CEACAM1. This resulted from the increased coupling of Shc to EGFR when its reciprocal sequestration by CEACAM1 was absent [33], as with respect to VEGFR [48] and the insulin receptor [32]. Thus, activation of NF-κB and the MAPK pathways downstream of these growth factor receptors constitutes a unifying mechanism underlying hepatic fibrosis when their shared substrate, CEACAM1, is lost. This agrees with the reported PPARβ/δ-driven HSCs proliferation and hepatic fibrosis via activation of the P38-JNK MAPK pathway in LX2 and murine HSCs [8].

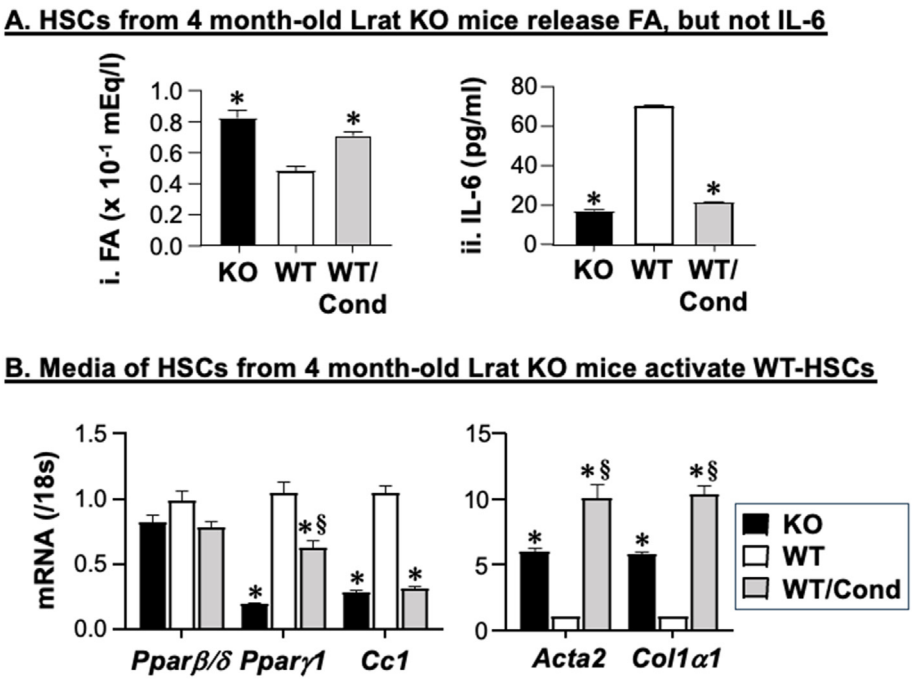

Figure 8: HSCs from 4-month-old *LratCre* + *Cc1*$^{fl/fl}$ mice activate wild-type HSCs. Primary HSCs were isolated from *LratCre* + *Cc1*$^{fl/fl}$ mice (KO; n = 8) and WT controls (n = 15); all at 4 months of age. On day 5, media was switched to phenol-free DMEM-10%FBS for another 24 h at which point conditioned (Cond) media from KO cells was collected and transferred to some WT cells (WT/Cond) for 24 h. (A) FA and IL-6 content in media was collected and (B) cells were harvested to assess mRNA levels by qRT-PCR in triplicate relative to 18s. Values are expressed as mean ± SEM; $^{*}P < 0.05$ vs WT and $^{\S}P < 0.05$ WT/Cond vs KO.

EGFR is implicated in HSCs activation [34,49] as demonstrated by the reversal of hepatic fibrogenesis, hepatocyte proliferation and liver injury in experimental models of hepatic fibrosis by inhibitors of EGFR tyrosine kinase activity [50,51]. Yet, inhibiting EGFR phosphorylation to curb hepatic fibrosis has not gained traction at the clinical setting. Instead, targeting inflammation and lipogenesis constitutes the main current therapeutic approach, particularly at the early stages of the disease [2,3]. This includes the use of a combinational therapy of PPARγ agonists and incretins to retard/attenuate hepatic fibrosis in patients with MASLD/MASH [52]. It is likely that the effectiveness of these drugs is mediated, at least partly, by the transcriptional activation of CEACAM1 [16], which would in turn, counter inflammation in immune cells [53] and lipogenesis in hepatocytes (by inhibiting FASN and limiting chronic hyperinsulinemia).

We have previously shown that hepatic CEACAM1 expression is progressively reduced with advancing fibrosis stages in patients with MASH [15]. Moreover, single cell RNA-sequencing showed lower CEACAM1 expression in hepatocytes and LSECs of patients with fibrosis/cirrhosis [17]. The current study demonstrated that activation of primary human HSCs repressed *CEACAM1* expression and that deleting *CEACAM1* from immortalized human LX2 activated them. The hepatic fibrosis phenotype of *LratCre* + *Cc1*$^{fl/fl}$ mutants concurrent to inflammatory infiltration to their liver parenchyma and the ability of their HSCs to cause fibrosis even at a young age in the absence of inflammatory effectors, further emphasized the regulation of hepatic fibrosis by CEACAM1's loss in HSCs, independently of its paracrine role in other liver cells. The underlying mechanisms converge at the level of NF-κB inflammation and MAPK proliferation pathways downstream of EGFR in HSCs (and in hepatocytes at the basal state) and of VEGFR in endothelial cells. Consistent with elevated serum IL-6 levels in patients with advanced hepatic fibrosis [54], loss of CEACAM1 in HSCs caused an elevation in plasma IL-6 levels concurrently wth hepatic fibrosis in *LratCre* + *Cc1*$^{fl/fl}$ mutants. Together, this proposes that inducing CEACAM1 expression could constitute an effective therapeutic approach to curb fibrosis, not only in early stages of the disease, but also at a later stage.

In summary, the current report provides an *in vivo* demonstration of a novel mechanistic link between a distinct CEACAM1/EGFR/NF-κB signaling module in murine HSCs and hepatic fibrosis, an advanced component of MASH. This was supported by studies in human LX2 HSCs demonstrating an autocrine regulation of hepatic fibrosis by the loss of CEACAM1 in stellate cells. Further analysis is required to translate our observations to MASH pathogenesis in humans.

CREDIT AUTHORSHIP CONTRIBUTION STATEMENT

Harrison T. Muturi: Writing — original draft, Validation, Methodology, Investigation, Formal analysis, Data curation. **Hilda E. Ghadieh:** Writing — original draft, Methodology, Investigation, Formal analysis, Data curation. **Suman Asalla:** Writing — original draft, Methodology, Investigation, Formal analysis, Data curation. **Sumona G. Lester:** Formal analysis, Data curation. **Getachew D. Belew:** Writing — review & editing, Methodology, Investigation, Data curation, Formal analysis. **Sobia Zaidi:** Data curation, Investigation. **Raziyeh Abdolahipour:** Methodology, Data curation. **Abhishek P. Shrestha:** Data curation, Formal analysis, Investigation. **Agnes O. Portuphy:** Investigation. **Hannah L. Stankus:** Methodology. **Raghd Abu Helal:** Investigation. **Stefaan Verhulst:** Investigation, Formal analysis, Data curation. **Sergio Duarte:** Data curation, Formal analysis. **Ali Zarrinpar:** Formal analysis, Data curation, Investigation. **Leo A. van Grunsven:** Writing — review & editing, Formal analysis, Data curation. **Scott L. Friedman:** Writing — review & editing, Validation, Methodology. **Robert F. Schwabe:** Writing — review & editing, Formal analysis, Data curation. **Terry D. Hinds:** Writing — review & editing, Formal analysis, Data

curation. **Sivarajan Kumarasamy:** Investigation. **Sonia M. Najjar:** Writing – review & editing, Validation, Supervision, Resources, Project administration, Investigation, Funding acquisition, Formal analysis, Conceptualization.

ACKNOWLEDGMENTS

S.M.N. is partly supported by the Osteopathic Heritage Foundation J.J.Kopchick, PhD Eminent Research Chair.

DECLARATION OF COMPETING INTEREST

None declared.

DATA AVAILABILITY

Data will be made available on request.

FINANCIAL SUPPORT

This work was supported by NIH grants: R01-DK054254 and R01-DK124126 (to S.M.N), R01-DK128289 (to S.L.F). S.V. is supported by FWO 1243121 N, and L.A.vG. by FWO G071922N.

APPENDIX A. SUPPLEMENTARY DATA

Supplementary data to this article can be found online at https://doi.org/10.1016/j.molmet.2024.102010.

REFERENCES

[1] Younossi ZM. Non-alcoholic fatty liver disease - a global public health perspective. J Hepatol 2019;70(3):531–44.
[2] Harrison SA, Allen AM, Dubourg J, Noureddin M, Alkhouri N. Challenges and opportunities in NASH drug development. Nat Med 2023;29(3):562–73.
[3] Wang S, Friedman SL. Found in translation-Fibrosis in metabolic dysfunction-associated steatohepatitis (MASH). Sci Transl Med 2023;15(716):eadi0759.
[4] Brunt EM, Kleiner DE, Carpenter DH, Rinella M, Harrison SA, Loomba R, et al. NAFLD: reporting histologic findings in clinical practice. Hepatology 2021;73(5):2028–38.
[5] Friedman SL. Mechanisms of hepatic fibrogenesis. Gastroenterology 2008;134(6):1655–69.
[6] Jophlin LL, Koutalos Y, Chen C, Shah V, Rockey DC. Hepatic stellate cells retain retinoid-laden lipid droplets after cellular transdifferentiation into activated myofibroblasts. Am J Physiol Gastrointest Liver Physiol 2018;315(5):G713–21.
[7] Hellemans K, Michalik L, Dittie A, Knorr A, Rombouts K, De Jong J, et al. Peroxisome proliferator-activated receptor-beta signaling contributes to enhanced proliferation of hepatic stellate cells. Gastroenterology 2003;124(1):184–201.
[8] Kostadinova R, Montagner A, Gouranton E, Fleury S, Guillou H, Dombrowicz D, et al. GW501516-activated PPARbeta/delta promotes liver fibrosis via p38-JNK MAPK-induced hepatic stellate cell proliferation. Cell Biosci 2012;2(1):34.
[9] Berry DC, Noy N. All-trans-retinoic acid represses obesity and insulin resistance by activating both peroxisome proliferation-activated receptor beta/delta and retinoic acid receptor. Mol Cell Biol 2009;29(12):3286–96.
[10] Forman BM, Chen J, Evans RM. Hypolipidemic drugs, polyunsaturated fatty acids, and eicosanoids are ligands for peroxisome proliferator-activated receptors alpha and delta. Proc Natl Acad Sci USA 1997;94(9):4312–7.
[11] Friedman SL. Hepatic fibrosis and cancer: the silent threats of metabolic syndrome. Diabetes Metab J 2024;48(2):161–9.
[12] DeAngelis AM, Heinrich G, Dai T, Bowman TA, Patel PR, Lee SJ, et al. Carcinoembryonic antigen-related cell adhesion molecule 1: a link between insulin and lipid metabolism. Diabetes 2008;57(9):2296–303.
[13] Ghadieh HE, Russo L, Muturi HT, Ghanem SS, Manaserh IH, Noh HL, et al. Hyperinsulinemia drives hepatic insulin resistance in male mice with liver-specific Ceacam1 deletion independently of lipolysis. Metabolism 2019;93:33–43.
[14] Helal RA, Russo L, Ghadieh HE, Muturi HT, Asalla S, Lee AD, et al. Regulation of hepatic fibrosis by carcinoembryonic antigen-related cell adhesion molecule 1. Metabolism 2021;121:154801.
[15] Zaidi S, Asalla S, Muturi HT, Russo L, Abdolahipour R, Belew GD, et al. Loss of CEACAM1 in hepatocytes causes hepatic fibrosis. Eur J Clin Invest 2024;54(7):e14177.
[16] Ghadieh HE, Muturi HT, Russo L, Marino CC, Ghanem SS, Khuder SS, et al. Exenatide induces carcinoembryonic antigen-related cell adhesion molecule 1 expression to prevent hepatic steatosis. Hepatol. Commun Now 2018;2(1):35–47.
[17] Muturi HT, Ghadieh HE, Abdolahipour R, Stankus HL, Belew GD, Liu JK, et al. Loss of CEACAM1 in endothelial cells causes hepatic fibrosis. Metabolism 2023;144:155562.
[18] Rueckschloss U, Kuerten S, Ergun S. The role of CEA-related cell adhesion molecule-1 (CEACAM1) in vascular homeostasis. Histochem Cell Biol 2016;146(6):657–71.
[19] El Taghdouini A, Sorensen AL, Reiner AH, Coll M, Verhulst S, Mannaerts I, et al. Genome-wide analysis of DNA methylation and gene expression patterns in purified, uncultured human liver cells and activated hepatic stellate cells. Oncotarget 2015;6(29):26729–45.
[20] Mederacke I, Hsu CC, Troeger JS, Huebener P, Mu X, Dapito DH, et al. Fate tracing reveals hepatic stellate cells as dominant contributors to liver fibrosis independent of its aetiology. Nat Commun 2013;4:2823.
[21] El Taghdouini A, Najimi M, Sancho-Bru P, Sokal E, van Grunsven LA. In vitro reversion of activated primary human hepatic stellate cells. Fibrogenesis Tissue Repair 2015;8:14.
[22] Mederacke I, Dapito DH, Affo S, Uchinami H, Schwabe RF. High-yield and high-purity isolation of hepatic stellate cells from normal and fibrotic mouse livers. Nat Protoc 2015;10(2):305–15.
[23] Schiffer E, Housset C, Cacheux W, Wendum D, Desbois-Mouthon C, Rey C, et al. Gefitinib, an EGFR inhibitor, prevents hepatocellular carcinoma development in the rat liver with cirrhosis. Hepatology 2005;41(2):307–14.
[24] Hinds Jr TD, Stechschulte LA, Cash HA, Whisler D, Banerjee A, Yong W, et al. Protein phosphatase 5 mediates lipid metabolism through reciprocal control of glucocorticoid receptor and peroxisome proliferator-activated receptor-gamma (PPARgamma). J Biol Chem 2011;286(50):42911–22.
[25] Ramakrishnan SK, Khuder SS, Al-Share QY, Russo L, Abdallah SL, Patel PR, et al. PPARalpha (peroxisome proliferator-activated receptor alpha) activation reduces hepatic CEACAM1 protein expression to regulate fatty acid oxidation during fasting-refeeding transition. J Biol Chem 2016;291(15):8121–9.
[26] Tsuchida T, Friedman SL. Mechanisms of hepatic stellate cell activation. Nat Rev Gastroenterol Hepatol 2017;14(7):397–411.
[27] Testerink N, Ajat M, Houweling M, Brouwers JF, Pully VV, van Manen HJ, et al. Replacement of retinyl esters by polyunsaturated triacylglycerol species in lipid droplets of hepatic stellate cells during activation. PLoS One 2012;7(4):e34945.
[28] Sauvant P, Cansell M, Atgie C. Vitamin A and lipid metabolism: relationship between hepatic stellate cells (HSCs) and adipocytes. J Physiol Biochem 2011;67(3):487–96.
[29] Tuohetahuntila M, Molenaar MR, Spee B, Brouwers JF, Wubbolts R, Houweling M, et al. Lysosome-mediated degradation of a distinct pool of lipid droplets during hepatic stellate cell activation. J Biol Chem 2017;292(30):12436–48.

[30] Tuohetahuntila M, Spee B, Kruitwagen HS, Wubbolts R, Brouwers JF, van de Lest CH, et al. Role of long-chain acyl-CoA synthetase 4 in formation of polyunsaturated lipid species in hepatic stellate cells. Biochim Biophys Acta 2015;1851(2):220–30.
[31] Wobser H, Dorn C, Weiss TS, Amann T, Bollheimer C, Buttner R, et al. Lipid accumulation in hepatocytes induces fibrogenic activation of hepatic stellate cells. Cell Res 2009;19(8):996–1005.
[32] Poy MN, Ruch RJ, Fernstrom MA, Okabayashi Y, Najjar SM. Shc and CEACAM1 interact to regulate the mitogenic action of insulin. J Biol Chem 2002;277(2):1076–84.
[33] Abou-Rjaily GA, Lee SJ, May D, Al-Share QY, Deangelis AM, Ruch RJ, et al. CEACAM1 modulates epidermal growth factor receptor–mediated cell proliferation. J Clin Invest 2004;114(7):944–52.
[34] Bhushan B, Michalopoulos GK. Role of epidermal growth factor receptor in liver injury and lipid metabolism: emerging new roles for an old receptor. Chem Biol Interact 2020;324:109090.
[35] She H, Xiong S, Hazra S, Tsukamoto H. Adipogenic transcriptional regulation of hepatic stellate cells. J Biol Chem 2005;280(6):4959–67.
[36] Ganji SH, Kashyap ML, Kamanna VS. Niacin inhibits fat accumulation, oxidative stress, and inflammatory cytokine IL-8 in cultured hepatocytes: impact on non-alcoholic fatty liver disease. Metabolism 2015;64(9):982–90.
[37] Zhou E, Li Y, Yao M, Wei Z, Fu Y, Yang Z. Niacin attenuates the production of pro-inflammatory cytokines in LPS-induced mouse alveolar macrophages by HCA2 dependent mechanisms. Int Immunopharm 2014;23(1):121–6.
[38] Wang Y, van Boxel-Dezaire AH, Cheon H, Yang J, Stark GR. STAT3 activation in response to IL-6 is prolonged by the binding of IL-6 receptor to EGF receptor. Proc Natl Acad Sci USA 2013;110(42):16975–80.
[39] Ueda A, Ishigatsubo Y, Okubo T, Yoshimura T. Transcriptional regulation of the human monocyte chemoattractant protein-1 gene. Cooperation of two NF-kappaB sites and NF-kappaB/Rel subunit specificity. J Biol Chem 1997;272(49):31092–9.
[40] Roca H, Varsos ZS, Sud S, Craig MJ, Ying C, Pienta KJ. CCL2 and interleukin-6 promote survival of human CD11b+ peripheral blood mononuclear cells and induce M2-type macrophage polarization. J Biol Chem 2009;284(49):34342–54.
[41] Tacke F. Targeting hepatic macrophages to treat liver diseases. J Hepatol 2017;66(6):1300–12.
[42] Quero L, Tiaden AN, Hanser E, Roux J, Laski A, Hall J, et al. miR-221-3p drives the shift of M2-macrophages to a pro-inflammatory function by suppressing JAK3/STAT3 activation. Front Immunol 2019;10:3087.
[43] Giannandrea M, Parks WC. Diverse functions of matrix metalloproteinases during fibrosis. Dis. Model Mech. 2014;7(2):193–203.
[44] Sun X, Harris EN. New aspects of hepatic endothelial cells in physiology and nonalcoholic fatty liver disease. Am J Physiol Cell Physiol 2020;318(6):C1200–13.
[45] Najjar SM, Yang Y, Fernstrom MA, Lee SJ, Deangelis AM, Rjaily GA, et al. Insulin acutely decreases hepatic fatty acid synthase activity. Cell Metabol 2005;2(1):43–53.
[46] O'Farrell M, Duke G, Crowley R, Buckley D, Martins EB, Bhattacharya D, et al. FASN inhibition targets multiple drivers of NASH by reducing steatosis, inflammation and fibrosis in preclinical models. Sci Rep 2022;12(1):15661.
[47] Li J, Bessho K, Shivakumar P, Mourya R, Mohanty SK, Dos Santos JL, et al. Th2 signals induce epithelial injury in mice and are compatible with the biliary atresia phenotype. J Clin Invest 2011;121(11):4244–56.
[48] Abu Helal R, Muturi HT, Lee AD, Li W, Ghadieh HE, Najjar SM. Aortic fibrosis in insulin-sensitive mice with endothelial cell-specific deletion of Ceacam1 gene. Int J Mol Sci 2022;23(8).
[49] Wan S, Liu X, Sun R, Liu H, Jiang J, Wu B. Activated hepatic stellate cell-derived Bmp-1 induces liver fibrosis via mediating hepatocyte epithelial-mesenchymal transition. Cell Death Dis 2024;15(1):41.
[50] Fuchs BC, Hoshida Y, Fujii T, Wei L, Yamada S, Lauwers GY, et al. Epidermal growth factor receptor inhibition attenuates liver fibrosis and development of hepatocellular carcinoma. Hepatology 2014;59(4):1577–90.
[51] Wang D, Xu H, Fan L, Ruan W, Song Q, Diao H, et al. Hyperphosphorylation of EGFR/ERK signaling facilitates long-term arsenite-induced hepatocytes epithelial-mesenchymal transition and liver fibrosis in sprague-dawley rats. Ecotoxicol Environ Saf 2023;249:114386.
[52] Wong VWS, Zelber-Sagi S, Cusi K, Carrieri P, Wright E, Crespo J, et al. Management of NAFLD in primary care settings. Liver Int 2022;42(11):2377–89.
[53] Horst AK, Najjar SM, Wagener C, Tiegs G. CEACAM1 in liver injury, metabolic and immune regulation. Int J Mol Sci 2018;19(10).
[54] Gunes A, Schmitt C, Bilodeau L, Huet C, Belblidia A, Baldwin C, et al. IL-6 trans-signaling is increased in diabetes, impacted by glucolipotoxicity, and associated with liver stiffness and fibrosis in fatty liver disease. Diabetes 2023;72(12):1820–34.

